

Superamphiphobic Surfaces with Controllable Adhesion Fabricated by Femtosecond Laser Bessel Beam on PTFE

Dongkai Chu, Subhash C. Singh, Jiale Yong, Zhibing Zhan, Xiaoyan Sun, Ji-An Duan, and Chunlei Guo*

In this study, a facile method is presented to fabricate superamphiphobic surfaces with controllable adhesion on polytetrafluoroethylene (PTFE), for the first time, using femtosecond laser Bessel beam. Compared to previous structures mostly based on 1D microstructure produced by Gaussian beam, the surfaces are characterized by highly uniform 2D periodic hill-groove structures covered with extensive porous-mesh nanostructures. Most significantly, the 2D hill-groove structures have a very high-aspect-ratio since the energy distribution of the Bessel beam is more uniform over a longer focusing range. Moreover, the profile of the obtained microstructures is a nearly perfect semi-spherical shape. As a result, the processed surfaces become superamphiphobic, exhibiting a contact angle of 166° for water and 160° for oil, respectively. Furthermore, the surface adhesion can be controlled from ultralow to ultrahigh by adjusting the period of the hill-groove 2D-patterned structures. It is demonstrated that the ultralow adhesion surfaces show excellent antifog and anti-icing properties, while the ultrahigh adhesion surfaces can be used for water and oil collection. Both surfaces have a good mechanical stability and are stable over a wide range of temperatures. The superamphiphobic PTFE surfaces with tunable adhesion can be used for self-cleaning, microfluidic systems, and harsh environments.

for creating functional bioinspired surfaces.^[1–5] Such superhydrophobic surfaces are usually characterized by a static contact angle (SCA) greater than 150°. The potential applications of these surfaces include separation of oil and water,^[6] protection of electronic devices,^[7] and adjusting cell/substrate adhesion in biomedicine.^[8] In contrast to superhydrophobic surfaces, superoleophobic surfaces are more complicated, but they can repel many organic with lower surface tension.^[9] Recently, superamphiphobic surfaces with both superhydrophobic and superoleophobic wettabilities have gained increasing attention due to their wide range of applications including corrosion resistance,^[10,11] antifouling,^[12] anti-icing,^[13,14] and drag-reduction.^[15] A number of methods have been demonstrated to create superamphiphobic surfaces, including spraying, dip coating, layer-by-layer assembly, photolithography, and chemical vapor deposition.^[16–20] However, the fabrication of superamphiphobic surfaces is still a major challenge, since these methods are complicated and the coatings are prone to

degradation. A robust and effective method is required to produce superamphiphobic surfaces.

A superamphiphobic surface, with ultrahigh SCA, but ultralow adhesion, is an ideal liquid-repellent surface. Liquid droplets on such surfaces can easily roll off even if the substrate is slightly tilted. Differently, the high-adhesion superamphiphobic surfaces can be useful in no loss microdroplets transportation.^[21,22] On ultrahigh adhesion surfaces, SCA of liquid droplets is usually above 150°, but droplets will stick to the surfaces and not roll off, even when the surfaces are upside down. Usually, the superamphiphobic surfaces are fabricated on materials, such as polydimethylsiloxane, fabrics, and aluminum. Unfortunately these materials may lose their superior wettability under harsh environments. Polytetrafluoroethylene (PTFE) has a very low surface energy and is a promising candidate for superamphiphobic surfaces. Moreover, PTFE is widely used in industry and daily life, due to its acid, alkali, and extreme temperature resistance.^[23,24] However, these properties also create challenges when fabricating micro/nanostructures on PTFE surfaces using traditional methods, such as thermal annealing and chemical etching.^[25] Currently, femtosecond (fs) laser with extremely high peak power and ultrashort pulse


1. Introduction

In nature, lotus leaves, springtails, fish, water strider feet, and butterflies wings exhibit unusual wetting behaviors of superhydrophobicity or superoleophobicity, providing ideal models

Dr. D. Chu, Dr. S. C. Singh, Dr. J. Yong, Dr. Z. Zhan, Prof. C. Guo
 The Institute of Optics
 University of Rochester
 Rochester, NY 14627, USA
 E-mail: guo@optics.rochester.edu

Dr. S. C. Singh, Prof. C. Guo
 The Guo China-U.S. Photonics Lab
 State Key Laboratory of Applied Optics (SKLAO)
 Changchun Institute of Optics, Fine Mechanics, and Physics
 Changchun 130033, P. R. China

Prof. X. Sun, Prof. J.-A. Duan
 State Key Laboratory of High Performance and Complex Manufacturing
 College of Mechanical and Electrical Engineering
 Central South University
 Changsha 410083, P. R. China

 The ORCID identification number(s) for the author(s) of this article can be found under <https://doi.org/10.1002/admi.201900550>.

DOI: 10.1002/admi.201900550

duration is widely applied in fabricating micro/nanostructures on various materials to obtain superhydrophobic and superoleophobic surfaces.^[26–29] It has been demonstrated that by using laser processing, adhesion-tunable superhydrophobic PTFE surfaces can be obtained.^[30] A superhydrophobic and superoleophobic PTFE surface with high contrast adhesion has also been reported.^[31] Previous works usually use a Gaussian beam to produce 1D microgrooves. However, it is difficult to fabricate high-aspect-ratio grooves using a Gaussian beam, due to its strong focusing that limits the longitudinal energy distribution. As a result, the obtained surfaces can only achieve either superhydrophobic surfaces with tunable adhesion or superamphiphobic surfaces with high adhesion.^[30,31] Compared to a Gaussian beam, a Bessel beam can maintain near constant profile over a longer distance. Furthermore, a Gaussian beam can suffer from nonlinear beam distortion when the laser intensity is higher than the ablation level, while a Bessel beam is immune to such instabilities.^[32,33] As a result, a Bessel beam is more suitable for processing high-aspect-ratio microgrooves on materials. However, surface structuring of PTFE has never been studied with fs laser Bessel beam.

In this paper, we fabricate superamphiphobic surfaces on PTFE with fs laser Bessel beam. Compared to previous structures which are mostly based on 1D microstructure,^[7,12,34,35] our structures are more complex, characterized by highly uniform 2D periodic high-aspect-ratio hill-groove structures covered with extensive porous-mesh nanostructures. In addition, due to the Bessel beam, the profile of these microstructures has a nearly perfect semi-spherical shape, rather than a pyramidal shape. It is shown that semi-spherical shapes have better water and oil repellent performance than pyramidal shapes. As a result, the processed surfaces become superamphiphobic, exhibiting SCA larger than 150° and sliding angle (SA) less than 10° for both water and edible oil. By changing the laser processing parameters the adhesion of the laser-treated surfaces can be tuned from ultralow to ultrahigh. The ultralow adhesion surfaces have both antifog and anti-icing properties, while the ultrahigh adhesion surfaces can collect water and oil droplets. In addition, the high-temperature tolerance of these superamphiphobic surfaces has been systematically studied.

2. Results and Discussion

Figure S1 in the Supporting Information shows the experimental setup used to process the PTFE sample. An industrial PTFE sheet with a thickness of 1 mm is mounted on a 2D translation stage with movement controlled by a computer. By using an axicon lens, the fs laser pulses are spatially shaped from a Gaussian beam to a Bessel beam. The fs laser Bessel beam is focused on the PTFE surface with a lens (focal length of 25.4 mm). In this experiment, the laser power is set constant at 500 mW. The period of the laser scanning lines is tuned by a control program. In contrast to a Gaussian beam, the Bessel beam has a more uniform energy distribution over a longer focusing range along the beam propagation direction, which means high-aspect-ratio grooves can be obtained, as shown in Figure S2 in the Supporting Information. The aspect ratio of the microgrooves fabricated by a Bessel beam increased

by a factor of 3.8 compared to the microgrooves fabricated by a Gaussian beam by using the same pulse energy and scanning speed. Moreover, during fs laser processing, the different focusing geometry of the beam will result in a different profile processed on the surface of the sample. This means that the morphologies of prepared microstructures depend on the laser spatial intensity distribution.^[32] Figure S1b,c in the Supporting Information shows the Gaussian beam and Bessel beam spatial intensity distribution, respectively. As a result, using the Bessel beam, the profile of the obtained structures has a nearly perfect semi-spherical shape (Figure 1b), rather than a pyramidal shape (Figure 1a). Figure 1c shows the water and oil contact angles between the Gaussian beam and Bessel beam processed surfaces. In both cases the Bessel beam produces better results; particularly, for oil, the surfaces processed by the Bessel beam show significantly better results, which can be attributed to the different micro/nanostructures processed by the different beams. Compared to previous structures which are mostly based on 1D microstructure,^[7,12,32,33] our structures are more complex. Figure 1d shows the scanning electron microscope (SEM) images of the prepared PTFE surfaces fabricated with a scanning speed of 1 mm s⁻¹. The surfaces are characterized by uniform 2D periodic high-aspect-ratio hill-groove structures covered with extensive nanostructures. The average width and depth of the grooves are about 50 and 60 μm, respectively. In contrast to the bare PTFE surface, the liquid repellence of the prepared PTFE surface is stable over a broad range of complex liquids, such as drinking water (72.8 mN m⁻¹), coffee (69.0 mN m⁻¹), milk (66.0 mN m⁻¹), glycerol (64 mN m⁻¹), vegetable oil (35 mN m⁻¹), and olive oil (32.5 mN m⁻¹). As shown in Figure 2, these liquids can easily slide down the prepared surfaces with a tilt of less than 10°. Figure 2b shows that the untreated sample is polluted by oil liquids, while the laser-treated sample maintains a clean state without any residual oil. This means the prepared surfaces have good antifouling characteristics. To measure the SCA and SA of the prepared surfaces, microsyringes are used to drop 6 μL water/oil droplets on the center of each surface. The prepared surface exhibits an SCA of 166° ± 1° for water and 160° ± 1.5° for edible oil, respectively, is an excellent superamphiphobic surface.

In contrast to previous structures which are mostly based on 1D microstructure,^[7,12,34,35] our 2D-patterned structures achieve better wettability. When droplet is in contact with the prepared surface, the 1D-patterned structures need a set of lines to hold the liquid droplet, while the 2D-patterned structures may need only several points, as shown in Figure S3a in the Supporting Information. Moreover, our 2D hill-groove structures show a high-aspect-ratio and are covered with numerous porous-mesh nanostructures, which are good superamphiphobic structures.

The scanning period shown in Figure 1d is a most crucial structure parameter, which has an important effect on the water/oil SCA and SA of the prepared surfaces. Figure 3a shows the typical laser confocal microscope images of the prepared surfaces with a period of 50 μm. With an increased period, the structures change from 2D-microdomes to 2D-microcubes, as shown in Figure 3b. The 2D-microcubes include the laser treated (structured) microgrooves and untreated (unstructured) square arrays. Figure 4 shows the relationships between the period and the SCA/SA of water and oil with volume of

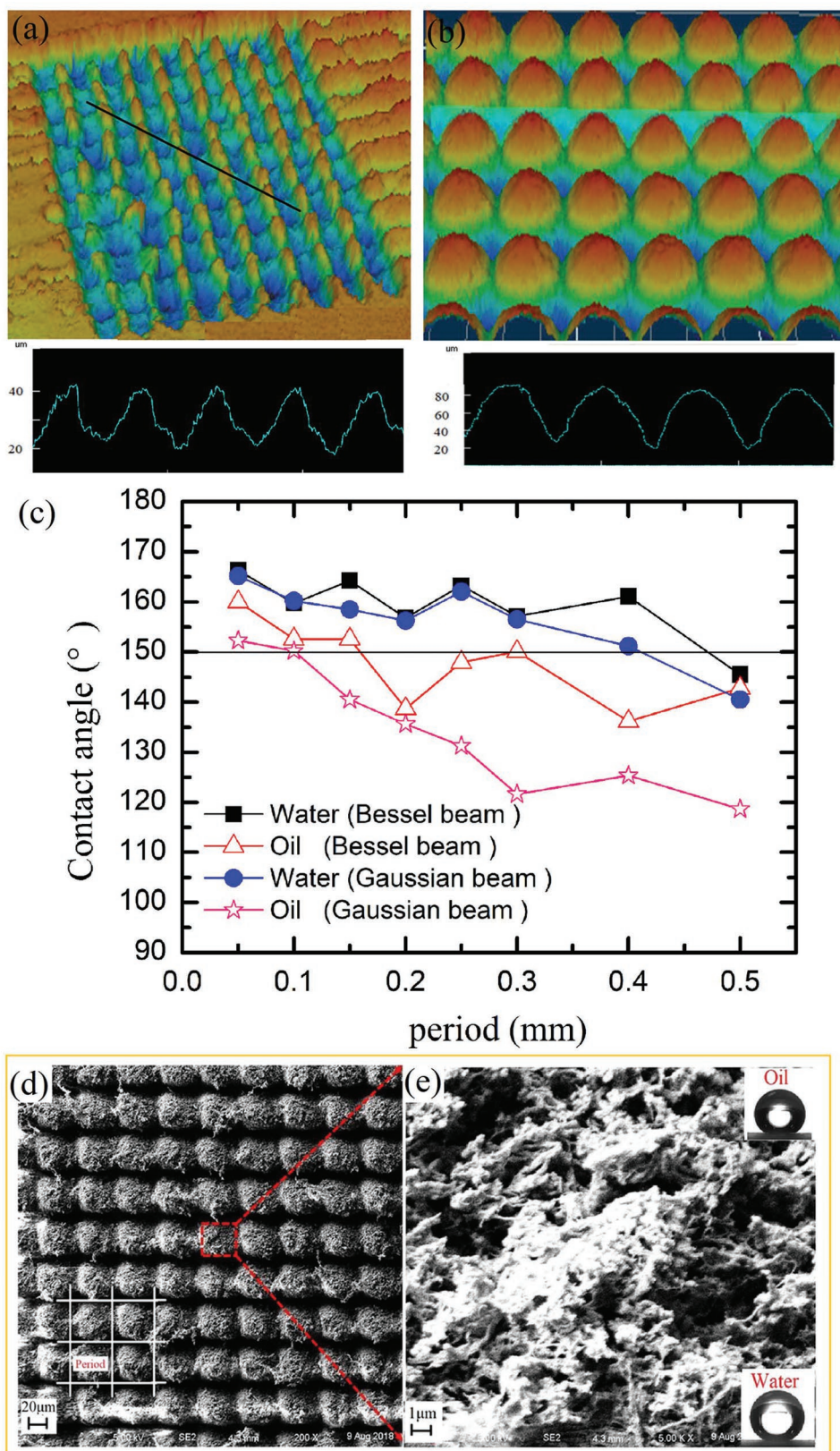


Figure 1. The surfaces treated by a) Gaussian beam and b) Bessel beam. c) Water and oil contact angle comparison between the Gaussian beam and Bessel beam. d) SEM images of prepared PTFE surfaces fabricated at the scanning speed of 1 mm s^{-1} . e) Large-magnification SEM image of the structure irradiated by fs laser pulses.

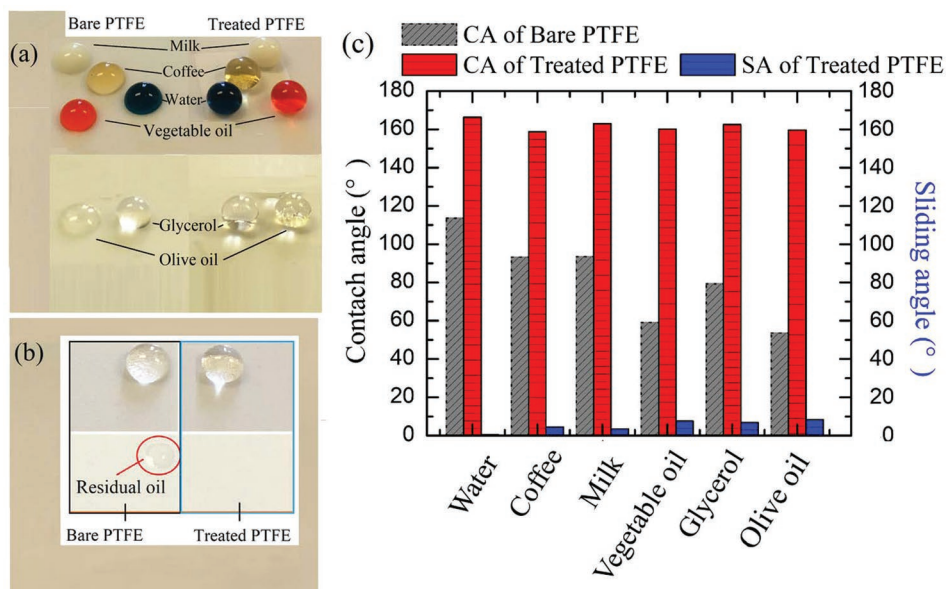


Figure 2. a) Optical photographs of water, vegetable oil, milk, coffee, glycerol, and olive oil drops on the untreated (left) and treated (right) PTFE. b) Comparison of the wettability of oil droplets on the untreated (left) and treated (right) PTFE surfaces. c) The SCA of bare PTFE and treated PTFE of different liquids droplets on the prepared surfaces, and the SA of the treated PTFE of different liquids droplets on the prepared surfaces.

6 μL). The result shows that the SCA of water and oil originally decreases with increasing period, while the SA sharply increases from almost 0° to 90° . Therefore by adjusting the period, the adhesion of the surface can be tuned from ultralow to ultrahigh, as shown in Figure 3c,d. The water/oil droplet from a microsyringe will remain suspended on the tip of the syringe, even after contact with the prepared surfaces with ultralow adhesion. This is done by having the microsyringe

with the water/oil droplet slowly approach the surface and then lift off after contact. The suspending water/oil droplet does not fall on the prepared surfaces (Movie S1, Supporting Information). This means that the prepared surface's adhesion is negligible. As the period increased to 200 μm , there are some untreated areas of the surfaces resulting in a higher adhesion than the treated surfaces. Consequently, the water/oil droplet will adhere to the surfaces, as shown in Figure 3d (Movie S2,

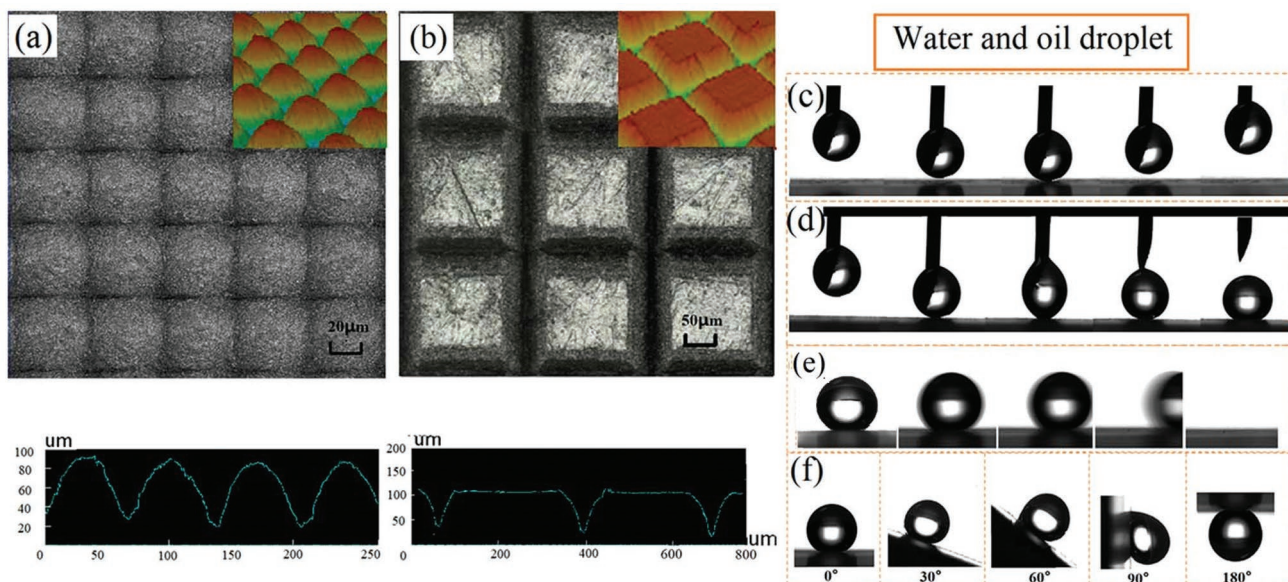


Figure 3. a) Laser confocal microscope image of prepared surfaces with different period: a) 50 μm and b) 200 μm . Water adhesion of the fs laser structured surfaces, photographs of a 6 μL water droplet contacting and leaving with the laser induced surfaces with period c) 50 μm and d) 200 μm . e) Time sequence of snapshots of an oil droplet rolling on the surfaces tilted 0.5° with period 50 μm . f) Prepared surfaces with period 200 μm at different angle tilted.

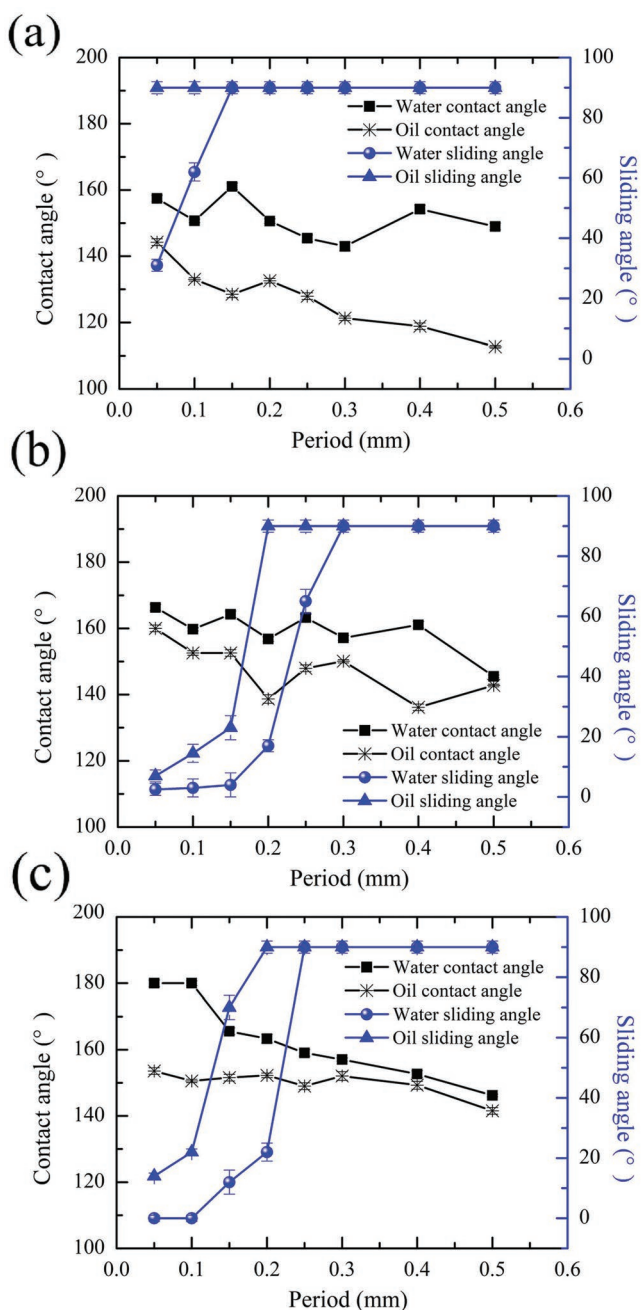


Figure 4. Relationships between the period and the water and oil SCA (left)/SA (right), respectively. The prepared surfaces are irradiated at a scanning speed a) 0.5 mm s⁻¹, b) 1 mm s⁻¹, and c) 2 mm s⁻¹, respectively.

Supporting Information). Furthermore, the water droplets can move very easily even when the prepared surfaces with ultralow adhesion are only slightly tilted or shaken (Figure 3e and Movie S3, Supporting Information). The oil droplets can also move when the prepared surface is tilted 7°. Besides SCA analysis, we also conduct water and oil advancing contact angle (ACA) and receding contact angle (RCA) tests for the prepared samples processed with scanning speed of 1 mm s⁻¹ and period of 50 μm, as shown in Figure S4 in the Supporting Information. The measurement method used is similar to ref. [36].

First, we carefully place a water drop of 6 μL volume on the prepared surface. Then we gradually tilt the surface and record a photo of the droplet using a high-resolution camera. We captured a photo right before the droplet started to move, as shown in Figure S4a in the Supporting Information. The hysteresis percentage can be described as [37]

$$\Delta\theta_{\%} = \frac{\cos\theta_{RCA} - \cos\theta_{ACA}}{2} \times 100\% \quad (1)$$

where θ_{RCA} and θ_{ACA} are the surfaces' RCA and ACA, respectively. According to Equation (1) and Figure S4 in the Supporting Information, the hysteresis percentage of the prepared surface is calculated to be 0.3% for water and 2.6% for oil. The hysteresis percentage for both water and oil is very low, which means that the adhesion of the prepared surface is ultralow. For the surface with ultrahigh adhesion, the water/oil droplets stick on the processed surfaces even if the surfaces are upside down (Figure 3f).

The underlying mechanism of the modulation of superamphiphobicity can be attributed to the unique chemical composition and the micro/nanostructure of the PTFE surface. It is well known PTFE has a very low surface energy (20 mN m⁻¹) due to its high content of -CF₂ groups. The surface tension of -CF₂ is lower than 6.7 mN m⁻¹. [38] Furthermore, the numerous porous-mesh nanostructures covered on the 2D-patterned microstructures can stabilize the gas absorbed in its concaves and provide a steady gas film. In addition, the microgroove processed by the fs laser Bessel beam shows a high-aspect-ratio, which allows the structures to trap more gas. Also due to different laser spatial intensity distribution between the Gaussian beam and Bessel beam (as shown in Figure S1b,c, Supporting Information), the profile of the obtained structures is a nearly perfect semi-spherical shape, rather than a pyramidal shape. When a liquid droplet is placed on the semi-spherical shape structured surface, a trapped air cushion will form between the droplets and the surface. As shown in Figure S4b in the Supporting Information, an array of convex liquid menisci in the downward direction will form between adjacent semi-spherical structures. The force exerted on the meniscus will be upright, pushing the liquid-air interface toward the top edge of the microdomes/cubes. In contrast, the pyramidal shape will exert a downward force, as discussed in ref. [39]. Therefore our structures exhibit superior repellent performance than the pyramidal shaped structures. As a result, the low surface energy groups combined with the high-aspect-ratio micro/nanostructure exhibit a strong repellence to water and oil, achieving superamphiphobicity. The adhesion of the prepared surfaces can be attributed to the change in the laser structured area and nonstructured domains. In contrast to structured surfaces, which show superamphiphobicity with ultralow water and oil adhesion, nonstructured surfaces shows ordinary amphiphobicity (as shown in Figure 2a) with ultrahigh water and oil adhesion. Therefore, the droplet on the structured surfaces exists in the Cassie state. The droplet is suspended by the gas layer trapped by the micro/nanoscale structures, resulting in a discontinuous three-phase contact line (TCL). This causes the adhesion of the surfaces to be extremely low making the droplets easily roll off. However, the droplets on the nonstructured surfaces will form a continuous TCL, which

can be considered to be the Wenzel or Young state. The droplets can wet the nonstructured surfaces completely, thus, ultrahigh water adhesion is observed. Accordingly, when the period is larger than 50 μm , the droplets on the surfaces generally exist in both the Cassie and Wenzel states. As the period increases, the contact state will slowly leave the Cassie state, leading to a decline in SCA. On the contrary, the SA will increase as the contact state moves into the Young state.

By comparing the SCA/SA of water and oil, using surfaces processed with different scanning speeds, we found that the optimal scanning speed to achieve superamphiphobic surfaces with ultralow adhesion is 1 mm s^{-1} , as shown in Figure 4b. Figure S5 in the Supporting Information shows the SEM images of processed surfaces prepared with different speeds. It can be clearly seen that the prepared surface is covered by microscale domes covered with extensive porous-mesh nanostructures. For water, when the scanning speed is increased, the density of nanostructures constantly increases, resulting in increased superhydrophobicity. Although when we put the 6 μL droplets on the prepared surfaces (processed with scanning speed of 2 mm s^{-1}) which were put on a calibrated platform, the droplet could not stabilize on the processed surface, as the Movie S4 in the Supporting Information shows. Therefore we estimate the SCA of the surfaces is approaching 180°. For oil, there is a scanning speed threshold of 1 mm s^{-1} . When the scanning speed is over the threshold, the depth of the microgrooves becomes smaller. The air filled percentage in the nanostructure and microstructure is too small to hold the oil (but it can hold water), allowing the oil to seep into the laser prepared area. Therefore, despite the increased density of the nanostructures, the SCA of the oil droplets decreased, as shown in Figure 4c.

High-temperature stability is the foundation of potential applications for the prepared samples. In this work, superamphiphobic surfaces under different temperatures are systematically studied. Figure 5a (Figure S6, Supporting Information) shows the relationship between temperatures and SCA/SA of water (Figure S6, Supporting Information, shows oil). It can be clearly seen that the SCA and SA of the prepared surfaces changed very little as temperature increased. Although the SCA is reduced slightly, it still exceeds 150°. SA is still less than 10°. Figure 5b,d shows the SEM images of the prepared surfaces before and after baking at 200 °C for 24 h. We can see that after high-temperature treatment, the nanostructures show little change. In the PTFE molecules, the C–C bond is covered by the F atom. The C and F atoms are joined by covalent bond. The energy of C–F bond is particularly stable. In addition, the $(\text{C}_2\text{F}_4)_n$ is a very large molecular group, a type of polymer. As a result, the surface can maintain high-temperature stability.

In order to test the mechanical properties of the prepared superamphiphobic PTFE sample, a bending test is conducted. After each bending, droplets are placed on the area where the bending occurred. Figure 6b shows water/oil SCA after each bending as a function of cycles. The water and oil SCA are all between 150° and 168°, indicating that superamphiphobic properties are retained even after 50 cycles.

The superamphiphobic PTFE surfaces, with ultralow or ultrahigh adhesion exhibit excellent antifog or water/oil collection properties, respectively, as shown in Figure 7. By exposing

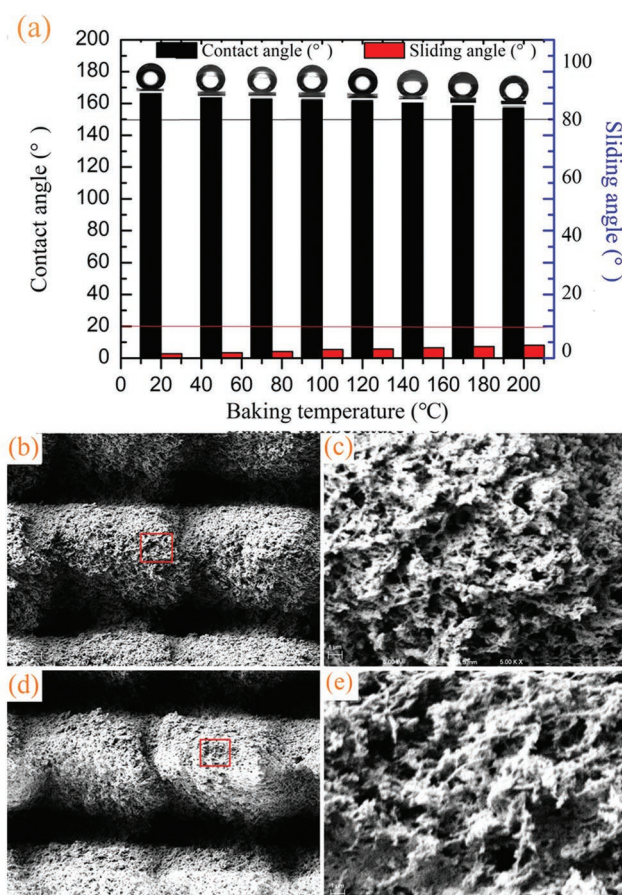


Figure 5. a) SCAs and SAs of water droplets on the prepared surfaces after heating with different temperature for 2 h. b–d) SEM images of the prepared surfaces b) before and d) after heating. Panels (c) and (e) show selected areas of (b) and (d) registered at a higher magnification.

the untreated and the treated PTFE samples to boiling water/oil steam, as shown in Figure 7e, the antifog and water/oil collection tests are conducted. Extensive amounts of tiny water/oil droplets form on the bare surfaces. Some of the larger droplets will attach onto the laser treated ultrahigh adhesive surface (white outline), which can be used for a water/oil collecting surfaces, shown in Figure 7c,d. Meanwhile the droplets cannot gather and conglutinate on the ultralow adhesion surface, achieving antifog property as shown in Figure 7a,b (black outline).

The superamphiphobic PTFE surface with ultralow adhesion additionally shows good anti-icing properties. During the anti-icing test, the bare sample and prepared samples with different adhesion are put into a freezer under conditions of $-10\text{ }^{\circ}\text{C}$ temperature and 60% humidity. After droplets are frozen (30 min), the samples are taken out. The ice droplets on the surface with ultrahigh/low adhesion are still in a spherical shape, as shown in Figure 8b. After placing the samples in a vertical orientation (as shown in Figure 8c) and slightly rocking them, interestingly, the ice easily sheds off from the laser treated surfaces with ultralow adhesion, while the ice remains on the surfaces with ultrahigh adhesion and the bare sample, shown in Figure 8c.

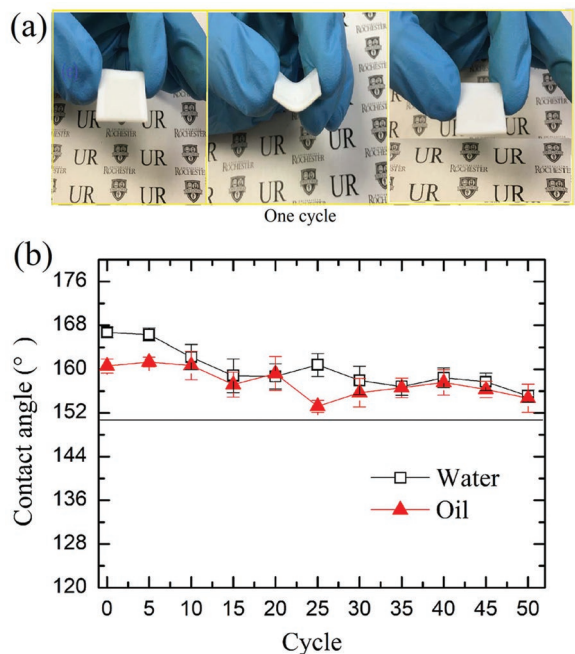


Figure 6. a) Bending test of the prepared surfaces. b) Water/oil CA after each bending as a function of cycles.

3. Conclusion

In conclusion, an effective approach to produce superamphiphobic surfaces with controllable adhesion is introduced by using fs laser Bessel beam processing. In contrast to previous structures mostly based on 1D microstructure and processed using a Gaussian beam, our surfaces show highly uniform 2D periodic hill-groove structures covered with extensive porous-mesh nanostructures. Specifically, our 2D hill-groove structures have a high-aspect-ratio. This is due to the Bessel beam having a more uniform energy distribution over a longer focusing range along the beam propagation direction than the Gaussian beam. In addition, due to the difference of the laser spatial intensity distribution between the Gaussian beam and the Bessel beam, the profile of the obtained structures is a nearly perfect semi-spherical shape, rather than a pyramidal shape. The semi-spherical shaped structures will excite an upward force to the water/oil droplets, driving liquid–air interface toward the top edges of the microdomes/cubes. The SCA of water and oil on these prepared surfaces can reach up to 166° and 160°, respectively, and the SA is 0.5° and 7°, respectively. Most importantly, the adhesion of the surfaces can be controlled from ultrahigh to ultralow by adjusting the period of the 2D-patterned structures. The fabricated surfaces with ultralow adhesion show good antifog and anti-icing properties,

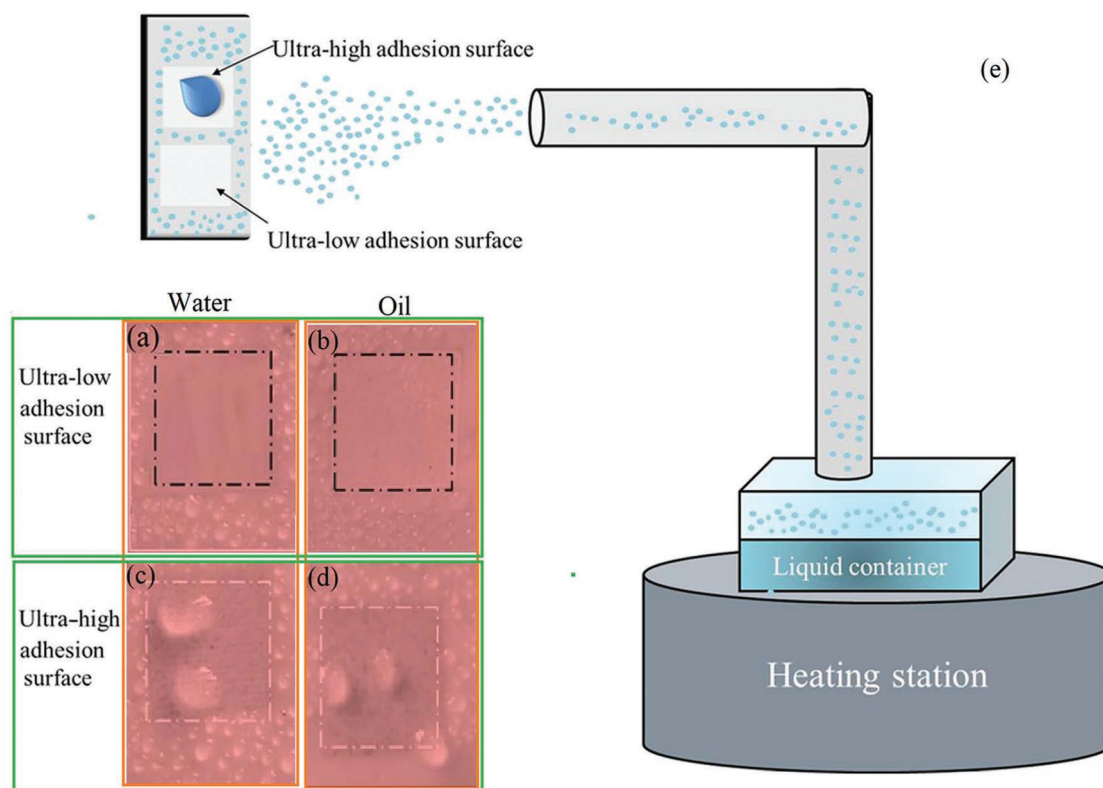


Figure 7. a–d) Antiwater/oil-fog property test: a,b) Ultralow adhesion surfaces for antiwater/oil-fog test. c,d) Ultrahigh adhesion surfaces for antiwater/oil-fog test. e) Antifog test setup. The white outline shows the fabricated surfaces with ultrahigh adhesion, while the black outline shows the surfaces with ultralow adhesion.

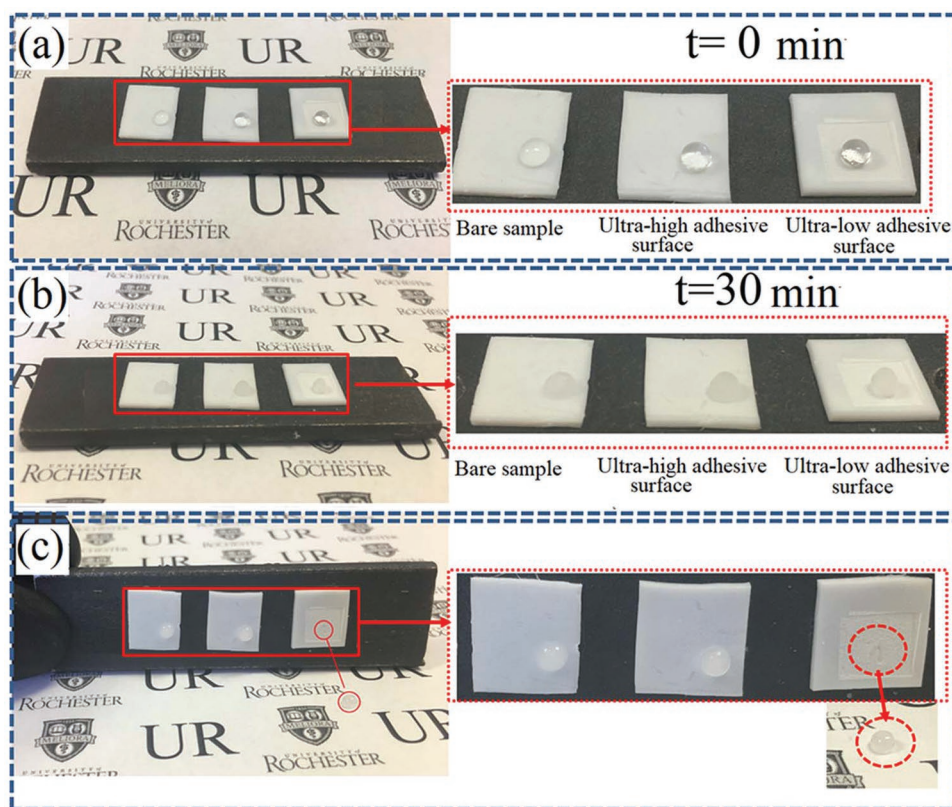


Figure 8. Anti-icing property test. a) Before and b) after place the sample in a refrigerator. c) The sample placed in a vertical orientation. The iced droplets on the bare sample and surface with ultrahigh adhesion are affixed but on the surface with ultralow adhesion the droplet falls off.

while the surfaces with ultrahigh adhesion can be used for water/oil collection. Both surfaces have a good mechanical stability and are able to sustain a wide range of temperature. The superamphiphobic PTFE surfaces with tunable adhesion can be used in antifouling, anti-icing, water/oil transport pipelines, and harsh environments.

4. Experimental Section

Materials: The industrial PTFE (Ligong, China) sheet with a thickness of 1 mm was purchased from Ligong Co. Ltd. The sheets are carefully rinsed with alcohol and distilled water before use. Distilled water and edible oil are used as the detecting water and oil, respectively.

Femtosecond Laser Processing: A Ti: sapphire regenerative amplifier laser system with pulses at a central wavelength of 800 nm, a pulse duration of 56 fs, and a repetition rate of 1 kHz was used. The fs laser beam is spatially shaped from a Gaussian beam to a Bessel beam by using an axicon lens. Usually, the intensity of the transformed Bessel beam is weak and not suitable for material processing. To increase the Bessel beam intensity, a 4f focusing system is used, resulting in a high quality Bessel beam with a significantly enhanced intensity. The laser beam is focused on the PTFE surfaces with a lens (focal length of 25.4 mm). The PTFE sheet is mounted on a 2D translation stage with movement controlled by a computer. A mechanical shutter is used, as a switch to pass or block the laser pulse. The laser energy incident on the sample is controlled by an attenuator that consists of a half-wave plate and a linear polarizer. After laser processing, the samples are cleaned with alcohol and deionized water in an ultrasonic bath at room temperature for 10 min each.

Characterization: The morphology of the superamphiphobic PTFE surfaces produced by fs laser pulses is obtained using a SEM (S-4100, Hitachi, Japan) and a laser confocal microscope (VK-9700, Keyence, Japan). Deionized water (surface tension of 72.8 mN m^{-1}) and edible oil (vegetable oil, the surface tension is about 35 mN m^{-1} , measured by hanging drop method) are used to investigate the wettabilities of both water and oil droplets on the prepared samples. The SCA and the SA are measured by a contact-angle system (SL2000KB, Kino, America). Microsyringes are used to drop $6 \mu\text{L}$ water/oil droplets on the center of each PTFE surface to measure the SCA and SA. The temperature tolerance of these samples is tested by an oven (Quincy lab, Inc, America, model 10 lab oven).

Supporting Information

Supporting Information is available from the Wiley Online Library or from the author.

Acknowledgements

The authors acknowledge financial supports from Bill and Melinda Gates Foundation (Grant No. OPP1119542), National Science Foundation (NSF, Grant No. IIP-1701163), and Chinses Scholarship Council (CSC).

Conflict of Interest

The authors declare no conflict of interest.

Keywords

Bessel beam, femtosecond laser, polytetrafluoroethylene, superamphiphobic surfaces, tunable adhesion

Received: March 27, 2019

Revised: May 15, 2019

Published online: June 7, 2019

- [1] F. Xia, L. Jiang, *Adv. Mater.* **2008**, *20*, 2842.
- [2] J. L. Yong, S. C. Singh, Z. B. Zhan, F. Chen, C. L. Guo, *Langmuir* **2019**, *35*, 921.
- [3] J. Genzer, A. Marmur, *MRS Bull.* **2008**, *33*, 742.
- [4] M. Liu, Y. Zheng, J. Zhai, L. Jiang, *Acc. Chem. Res.* **2010**, *43*, 368.
- [5] K. Yin, S. Yang, X. R. Dong, D. K. Chu, J. A. Duan, J. He, *Appl. Phys. Lett.* **2018**, *112*, 243701.
- [6] C. Wang, T. Yao, J. Wu, C. Ma, Z. Fan, Z. Wang, Y. Cheng, Q. Lin, B. Yang, *ACS Appl. Mater. Interfaces* **2009**, *1*, 2613.
- [7] L. Mishchenko, B. Hatton, V. Bahadur, J. A. Taylor, T. Krupenkin, J. Aizenberg, *ACS Nano* **2010**, *4*, 7699.
- [8] F. Shi, J. Niu, J. Liu, F. Liu, Z. Wang, X. Q. Feng, X. Zhang, *Adv. Mater.* **2007**, *19*, 2257.
- [9] D. Satam, H. J. Lee, E. Wilusz, *AATCC Rev.* **2010**, *10*, 59.
- [10] X. D. Zhang, P. Wu, Y. Y. Shen, L. H. Zhang, Y. H. Xue, F. Zhu, D. C. Zhang, C. L. Liu, *Appl. Surf. Sci.* **2011**, *258*, 151.
- [11] F. Zhang, L. Zhao, H. Chen, S. Xu, D. G. Evans, X. Duan, *Angew. Chem., Int. Ed.* **2008**, *47*, 2466.
- [12] J. Genzer, K. Efimenko, *Biofouling* **2006**, *22*, 339.
- [13] S. Farhadi, M. Farzaneh, S. A. Kulinich, *Appl. Surf. Sci.* **2011**, *257*, 6264.
- [14] J. Yang, W. Li, *J. Alloys Compd.* **2013**, *576*, 215.
- [15] C. Lee, C. J. Kim, *Phys. Rev. Lett.* **2011**, *106*, 014502.
- [16] R. Yuan, S. Wu, P. Yu, B. Wang, L. Mu, X. Zhang, Y. Zhu, B. Wang, H. Wang, J. Zhu, *ACS Appl. Mater. Interfaces* **2016**, *8*, 12481.
- [17] X. Wu, L. Wyman, G. Zhang, J. Lin, Z. Liu, Y. Wang, H. Hu, *Prog. Org. Coat.* **2016**, *90*, 463.
- [18] X. Zhou, Z. Zhang, X. Xu, F. Guo, X. Zhu, X. Men, B. Ge, *ACS Appl. Mater. Interfaces* **2013**, *5*, 7208.
- [19] H. Zou, S. Lin, Y. Tu, F. Li, J. Hu, G. Liu, S. Hu, G. Yang, Z. Yu, *Adv. Mater. Interfaces* **2016**, *3*, 1500693.
- [20] T. Wang, J. Cui, S. Ouyang, W. Cui, S. Wang, *Nanoscale* **2016**, *8*, 3031.
- [21] L. Feng, Y. N. Zhang, J. M. Xi, Y. Zhu, N. Wang, F. Xia, L. Jiang, *Langmuir* **2008**, *24*, 4114.
- [22] J. L. Yong, F. Chen, Q. Yang, D. S. Zhang, G. Q. Du, J. Si, H. F. Yun, X. Hou, *J. Phys. Chem. C* **2013**, *117*, 24907.
- [23] K. P. Adhi, R. L. Owings, T. A. Railkar, W. D. Brown, A. P. Malshe, *Appl. Surf. Sci.* **2003**, *218*, 17.
- [24] S. K. Biswas, K. Vijayan, *Wear* **1992**, *158*, 193.
- [25] Y. Li, E. J. Lee, S. O. Cho, *J. Phys. Chem. C* **2007**, *111*, 148137.
- [26] K. Yin, D. K. Chu, X. R. Dong, C. Wang, J. A. Duan, J. He, *Nanoscale* **2017**, *9*, 14229.
- [27] J. L. Yong, S. C. Singh, Z. B. Zhan, F. Chen, C. L. Guo, *ACS Appl. Mater. Interfaces* **2019**, *11*, 8667.
- [28] K. Yin, H. F. Du, X. R. Dong, C. Wang, J. A. Duan, J. He, *Nanoscale* **2017**, *9*, 14620.
- [29] J. A. Duan, X. R. Dong, K. Yin, S. Yang, D. K. Chu, *Appl. Phys. Lett.* **2018**, *113*, 203704.
- [30] Y. Fang, J. L. Yong, F. Chen, J. L. Huo, Q. Yang, H. Bian, G. Q. Du, X. Hou, *Appl. Phys. A* **2016**, *122*, 827.
- [31] X. J. Liu, W. C. Wu, X. L. Wang, Z. Z. Luo, Y. M. Liang, F. A. Zhou, *Soft Matter* **2009**, *5*, 3097.
- [32] Z. Luo, J. A. Duan, C. Cuo, *Opt. Lett.* **2017**, *42*, 2358.
- [33] M. K. Bhuyan, F. Courvoisier, P. A. Lacourt, M. Jacquot, R. Salut, L. Furfaro, J. M. Dudley, *Appl. Phys. Lett.* **2010**, *97*, 081102.
- [34] A. Y. Vorobyev, C. Guo, *J. Appl. Phys.* **2015**, *117*, 033103.
- [35] E. Fadeeva, S. Schlie, J. Koch, B. N. Chichkov, A. Y. Vorobyev, C. Guo, *Contact Angle, Wettability Adhes.* **2009**, *6*, 164.
- [36] F. Schellenberger, N. Encinas, D. Vollmer, H. J. Butt, *Phys. Rev. Lett.* **2016**, *116*, 096101.
- [37] J. T. Korhonen, T. Huhtamaki, O. Ikkala, R. H. A. Ras, *Langmuir* **2013**, *29*, 3858.
- [38] S. Yang, K. Yin, D. K. Chu, J. He, J. A. Duan, *Appl. Phys. Lett.* **2018**, *113*, 203701.
- [39] J. L. Yong, F. Chen, Q. Yang, J. L. Huo, X. Hou, *Chem. Soc. Rev.* **2017**, *46*, 4168.